11-2015

EXCESS MID-INFRARED FLUX: AN INDICATOR OF MASS LOSS IN CEPHEIDS?

Edward G. Schmidt
University of Nebraska-Lincoln, eschmidt1@unl.edu

The Astrophysical Journal, 813:29 (10pp), 2015 November 1 doi:10.1088/0004-637X/813/1/29

EXCESS MID-INFRARED FLUX: AN INDICATOR OF MASS LOSS IN CEPHEIDS?

Edward G. Schmidt
Department of Physics and Astronomy, University of Nebraska, Lincoln, NE, USA; eschmidt1@unl.edu
Received 2015 June 16; accepted 2015 September 23; published 2015 October 27

ABSTRACT

Spectral energy distributions for 132 classical and type II Cepheids were searched for evidence of excess flux above the photospheric level in the mid-infrared. Eight of them were found to have unambiguously strong excess emission while a further 13 showed evidence of weak emission. The presence of emission appears to be unrelated to either the pulsational amplitude or the effective temperature while strong emission is limited to stars with periods longer than 11 days, with a single exception. For the stars with strong emission we attempted to fit the energy distribution with a stellar wind model. No acceptable fit could be found for silicate grains. With graphite or iron grains we could only obtain an acceptable fit if the maximum dust temperature was significantly lower than the condensation temperature. We conclude that the excess emission is not evidence of mass loss.

Key words: stars: Population II – stars: variables: Cepheids

Supporting material: machine-readable table

1. INTRODUCTION

Mass loss in Cepheid variable stars is important to our understanding of both stellar evolution and the interactions between pulsation and mass loss. Most of the work on these issues has been concerned with the young, massive classical Cepheids while the old, low mass type II Cepheids have received little attention.

It has been suggested that the well-known mass discrepancy between evolutionary and pulsational masses for classical Cepheids might be attributed to mass loss (e.g., Kervella et al. 2009) while various investigators have considered the effect of pulsation on mass loss (e.g., Neilson & Lester 2008; Neilson et al. 2009, 2010). Neilsen et al. (2012) argued that mass loss must be widespread among Cepheids in order to reconcile observed period changes with evolutionary model predictions. Unfortunately, mass loss is difficult to measure observationally.

In the case of classical Cepheids, features with velocities close to escape velocity have been observed in some spectral lines including $H\alpha$ (Nardetto et al. 2008, and references there in), and Mg H and K (Schmidt & Parsons 1984; Deasey 1988; Bohm-Vitense & Love 1994). While this is suggestive of mass outflow, it is not definitive and is insufficient to calculate mass-loss rates.

If the outflow contains significant amounts of dust, its presence might be inferred from excess infrared emission. A number of investigators have analyzed infrared observations of classical Cepheids (Deasey & Butler 1986; McAlary & Welch 1986; Deasey 1988; Neilson & Lester 2008; Neilson et al. 2009, 2010) but only McAlary & Welch (1986) included results related to type II Cepheids. The latter paper concluded that classical Cepheids with significant mass loss are rather unusual while the majority of the seven type II Cepheids in their sample showed strong infrared emission. Given the low metallicities of many type II Cepheids, this is somewhat surprising.

Finally, circumstellar emission around some Cepheids that might (or might not) be related to mass loss has been reported based on near-infrared imagery or interferometry (e.g., Merand et al. 2006, 2007; Kervella et al. 2009; Marengo et al. 2010; Barmby et al. 2011) and VLA observations of neutral hydrogen (Matthews et al. 2012).

A more comprehensive review of observational evidence relating to circumstellar matter and mass loss in Cepheids can be found in Neilson & Lester (2008).

The availability of the mid-infrared photometry from the *Wide-field Infrared Survey Explorer* (*WISE*, Wright et al. 2010) offers the opportunity to revisit the infrared emission from Cepheids. In particular, it provides data from a larger sample of type II Cepheids. This paper presents the results of such a study of both classical and type II Cepheids.

2. THE SAMPLE

The stars discussed here include 60 type II Cepheid candidates identified by Schmidt (2013, Table 7) and 77 known Cepheids that we have observed previously (Schmidt et al. 2004, 2005a, 2005b). They are listed in Table 1 where the first column gives their designations from the General Catalog of Variable Stars or the Catalog of Suspected Variables (GCVS and NSV; with corrections and additions from the online version).[1] Since not all of the stars are yet in those catalogs, the preliminary designations from Schmidt et al. (2007, 2009) and Schmidt (2013) are given in column (2) for stars discussed in those papers. Column (3) indicates whether the stars were regarded as classical or type II Cepheids in our previous papers based on distance from the Galactic Plane (referred to here as *Z*-types).

The heterogeneity of the type II Cepheids can make it difficult to reliably distinguish them from other types of variables with similar periods. The AAVSO International Variable Star Index[2] (the VSX) gives classifications based on a variety of criteria and can provide a check on our classifications. They are listed in column (4) for stars in common (i.e., those with GCVS variable star names). For a majority of the stars the VSX types are consistent with their being classical Cepheids (VSX type DCEP), type II Cepheids (VSX types CWA, CWB, AHB1 or RVA), or Cepheids of uncertain type (VSX type CEP). However, five of them are listed in the VSX as EA/D/WD, BY, RS or UG. An examination of the original sources of these

[1] VizieR Online Data Catalog, II/250 and II/140.

[2] www.aavso.org/vsx. A description of the VSX types can be found by clicking on the "About" tab and selecting "Variability Types" at the bottom of that page.

Table 1
The Program Stars

Star	Prelim. Desig.	Z Type	VSX Type	Period	E_{B-V}	Source[a]	Emis. Cat.	Notes
(1)	(2)	(3)	(4)	(5) (days)	(6) (mag)	(7)	(8)	(9)
	B138	Type II	…	0.831	0.013	3	D	1
UY CrB	H091	Type II	CWB	0.929	0.034	3	D	1
BX Del	…	Type II	CWB	1.092	0.102	3	C	1
	A134	Type II	…	1.114	0.042	3	C	…
V0716 Oph	H093	Type II	AHB1	1.116	0.384	3	D	1

Notes.
[a] (1) Schmidt et al. (2011) or Schmidt (2013), (2) DDO Database or Fernie (1990), (3) Schlafly & Finkbeiner (2011).
[1] No W4 magnitude.
[2] No W3 or W4 magnitude.
[3] Companion may contribute to flux.
[4] Poor fit to VRJHK$_S$ fluxes.
[5] Rise beyond 10 μm.
[6] Infrared emission appears to overlap with the K$_S$ band.
[7] No W3 magnitude and W4 is very high. Probably no excess.

(This table is available in its entirety in machine-readable form.)

classifications showed that all are based either on spectra or detection as X-ray sources. Accordingly, these objects are not discussed here but are included for reference in Table 1.

Distinguishing between classical and type II Cepheids is often difficult. The *Z*-types and the VSX types agree as to whether individual stars are classical or type II Cepheids for 80% of the stars that have both classifications. It is often difficult to trace the origin of the VSX types. On the other hand, the *Z*-types will distinguish classical from type II Cepheids in most cases but there are certainly type II Cepheids near the Galactic Plane and possibly classical Cepheids at several scale heights from the Plane. Thus, the disagreement in the classifications for about a fifth of the sample is not unreasonable. This has little effect on the conclusions of this paper and when the statistics are discussed in Section 3.3, we will consider both classifications.

The periods of the stars are listed in column (5) while adopted reddenings, E_{B-V}, are given in column (6).

The reddenings were obtained from Schmidt et al. (2011) or Schmidt (2013), the David Dunlap Observatory Database of Galactic Classical Cepheids,[3] and Fernie (1990) in that order of preference. For the stars not found in any of these sources, reddenings were estimated from the extinction maps of Schlegel et al. (1998) as recalibrated by Schlafly & Finkbeiner (2011).[4] These reddenings are subject to uncertainties related to multiple assumptions used in making the maps (e.g., constant dust temperature along the line of sight, the calibration of column density in terms of E_{B-V}, and uniform dust properties) and to possible variations in the absorbing medium that are not resolved by the maps. Additionally, the maps give the total extinction along a line of sight through the Milky Way. This is a reasonable approximation of the foreground extinction to the type II stars since they are at relatively high latitude but may over-estimate the extinction for the classical Cepheids near the Galactic Plane. Consequently, we regard these values of extinction as being less reliable than those derived from the other methods and they are only used as a last resort. The source for each reddening is indicated in column (7) of Table 1.

Column (8) gives the emission category discussed below and column (9) contains references to the table footnotes.

Given the heterogeneity of the reddenings, they are not amenable to statistical analysis. Nonetheless, an intercomparison of stars in common between the various sources will give a rough idea of the uncertainties. The Fernie reddenings (all for classical Cepheids) were systematically larger than the Schmidt values by 0.09 $\pm$ 0.05 mag. The Schlafly and Fishbeiner excesses were systematically smaller than the Schmidt values by 0.05 $\pm$ 0.09 mag for the type II Cepheids and 0.21 $\pm$ 0.25 mag larger for the classical Cepheids. Thus, we will adopt an uncertainty of 0.25 mag in E_{B-V} (roughly encompassing the range of values) for the discussion below.

In this paper we have used the optical *V* and *R* magnitudes from our papers cited above, the near-infrared *J*, *H*, and K_S magnitudes from the Two Micron All Sky Survey (2MASS, Skrutskie et al. 2006) and the mid-infrared W1, W2, W3, and W4 magnitudes from the ALLWISE database. As indicated by a null entry for the magnitude error in the database, W4 is unreliable for many of the stars and the W3 measurement is unreliable for a few. Such magnitudes were omitted from the analysis and the affected stars are flagged by footnotes in Table 1. All the magnitudes were corrected for interstellar extinction using the reddenings listed in Table 1 and the extinction ratios of Fitzpatrick (1999).

3. EXCESS INFRARED EMISSION

We searched for excess emission in the mid-infrared using fluxes derived from the nine photometric magnitudes. Examples are plotted in Figures 1–4. We model the photospheric flux in the mid-infrared by fitting the spectral energy distributions (SEDs) from model atmospheres to the optical and near-infrared fluxes ($\lambda < 2.2$ μm). The models of Castelli & Kurucz (2003)[5] with log g = 2.5, [M/H] = 0, $v_{\rm turb}$ = 2.0 km s^{-1}, and 1/H = 1.25[6]

[3] www.astro.utoronto.ca/DDO/research/cepheids/
[4] Using the application at irsa.ipac.caltech.edu/applications/DUST/.
[5] Available at www.user.oats.inaf.it/castelli/grids.html.
[6] H is the mixing length in units of the pressure scale height of the atmosphere.

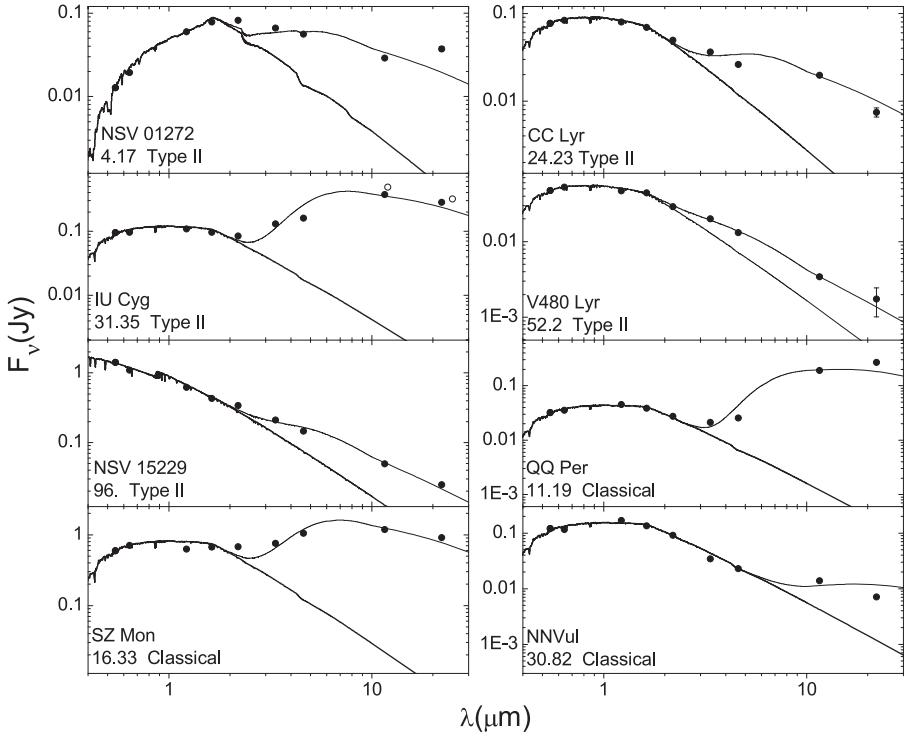

Figure 1. Spectral energy distributions of all the Cepheids with strong, unambigious excess infrared emission (category A). Filled circles represent the observed fluxes calculated from the broadband photometry. Error bars are plotted when they are larger than the symbols. In each panel, the darker curve is the fitted model atmosphere SED while the lighter curve is the sum of the photospheric SED and the SED that was fitted to the excess emission in the infrared. The fitting is discussed in Section 4 below. The star's name, its period in days, and its classification are given in the lower left corner of each panel. For IU Cyg, the two open circles represent fluxes from McAlary & Welch (1986).

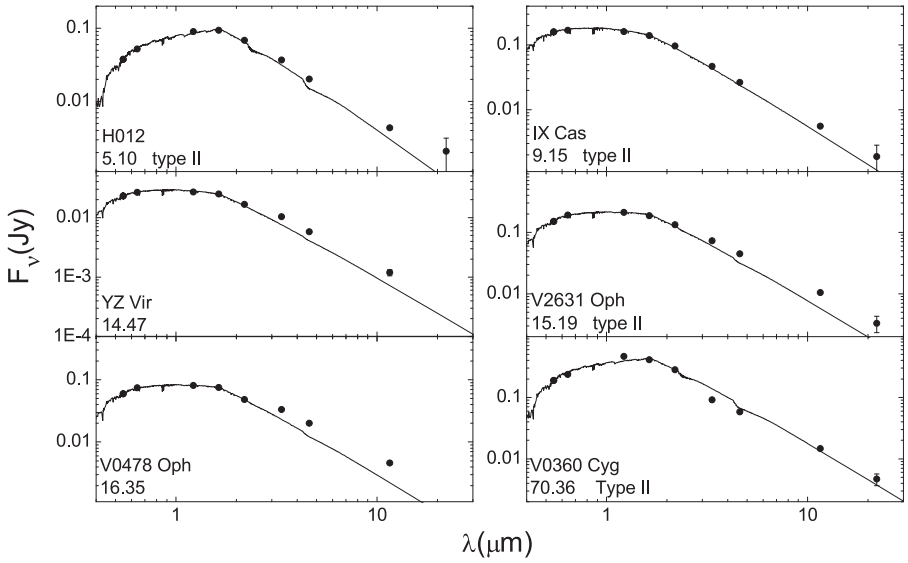

Figure 2. Spectral energy distributions for representative stars with weak mid-infrared excesses (category B). The symbols are the same as in Figure 1.

(denoted by fp00k2c125odfnew on the Castelli website) were adopted and the effective temperature, $T_{\rm eff}$, was determined from the fitting. The fitted model fluxes are shown in Figures 1–4 as solid lines. The excess emission will be recognized as mid-infrared fluxes that are above the fitted models.

3.1. Sources of Uncertainty

Before examining the SEDs to identify infrared excesses, we need to consider sources of uncertainty.

3.1.1. Contamination of the WISE Fluxes by Other Objects

To estimate the probability of contamination, we downloaded all of the objects from the *WISE* catalog between 45″ and 100″ from each program star.[7] These were then examined to determine how many were bright enough in the W3 band to cause the program star to be erronously identified as having

[7] Stars closer than 45″ of our program stars are generally not present in the *WISE* catalog. This is presumably because the photometry of these fainter objects is not reliable close to a relatively bright star.

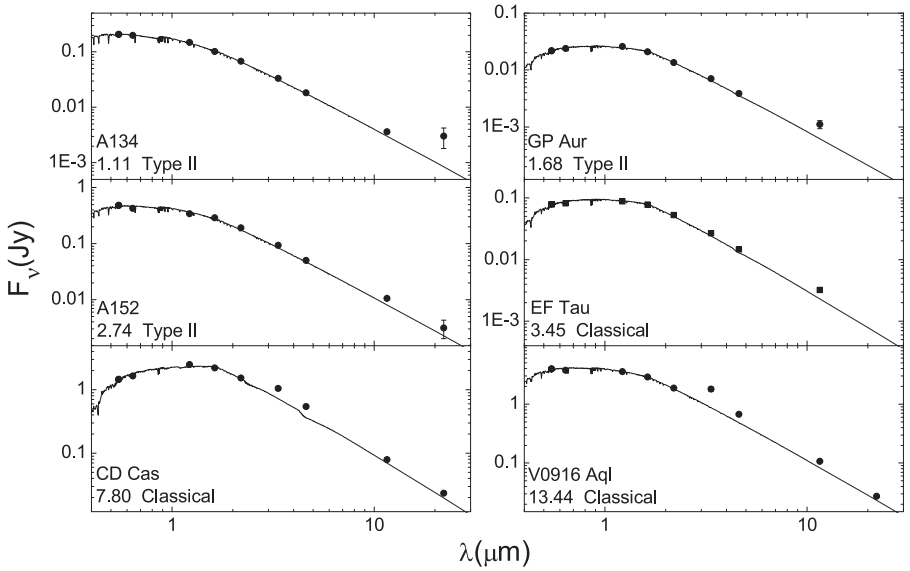

Figure 3. Spectral energy distributions for representative stars with anomalous mid-infrared fluxes (category C). The symbols are the same as in Figure 1.

excess mid-infrared emission (our category A or B defined below). Normalizing the count to the area of the *WISE* point-spread function (assuming a FWHM of 6″) gives the probability that the program star is contaminated by an unrelated field object. The largest probability for any individual star was less that 2.7%. Combining the probabilities for all of the program stars we find that there is slightly less than a 50% chance that one of our 132 Cepheids has been contaminated.

3.1.2. The Assumed Atmospheric Parameters

The atmospheric parameters of the models fitted to the observations were chosen rather arbitrarily to represent typical values obtained by Schmidt et al. (2011) and Schmidt (2013) for many of the present sample of stars. To test whether this affected the results we redid the fitting using models with log $g = 2.5$, [Fe/H] $= -1.0$ (i.e., the same gravity as but lower metallicity) and with log $g = 4.5$, [Fe/H] $= 0.0$ (same metallicity but higher gravity). An examination of the energy distributions showed differences that were comparable in size to the error bars for all nine filter bands. Thus, the assumption of the gravity and metallicity has no significant effect on the results.

3.1.3. Limited Phase Coverage

Ideally, all of the photometry for a single star should be obtained simultaneously or at least at the same pulsational phase. Unfortunately, such data do not exist. Nearly as good would be magnitudes derived from intensity means over the cycle. These are only available for the *VR* photometry.

The *JHK*$_S$ magnitudes from 2MASS are based on single epochs. Thus, the fluxes may be shifted up or down by as much as half of their amplitudes relative to the other fluxes. All three will be shifted in the same sense since the light curves are similar in shape and phase as can be seen by an inspection of the light curves of Welch et al. (1984).

The maximum J amplitude among galactic classical Cepheids listed by Inno et al. (2015, Table 2) is $A_J = 0.65$ suggesting that there should be shifts corresponding to as much as $\Delta J = \langle J \rangle - J_\phi \sim \pm 0.3$ mag where $\langle J \rangle$ refers to the intensity mean and J_ϕ is the magnitude at the phase of the observation. Larger amplitudes in the near-infrared have been reported for some type II Cepheids (e.g., Matsunaga et al. 2013) so we may expect to encounter a few larger values of ΔJ. The shifts for the other two filters will be $\Delta H = 0.76 \cdot \Delta J$, and $\Delta K_S = 0.72 \cdot \Delta J$ based on the relative amplitudes in those filter bands from the photometry of Welch et al. (1984).

At infrared wavelengths, the Rayleigh–Jeans law, with its $1/\lambda^2$ dependence, becomes a good approximation of the Planck function. This dependence carries over to the model SEDs except for a couple of minor molecular features around 2.4 μm and 4.5 μm (e.g., see NSV 01272 in Figure 1). In Figures 1–4 it can be seen that the model atmosphere SEDs are very nearly linear at wavelengths longer than 3 μm over the entire range of effective temperatures in our sample. This indicates that the Rayleigh–Jeans law is a good approximation in the mid-infrared for our stars. The JHK$_S$ bands lie in the region of transition to the Rayleigh–Jeans law. Hence, moving their fluxes up or down simply moves the fitted SED at longer wavelengths up or down relative to the *WISE* fluxes but does not alter its slope.

The observing strategy employed by the *WISE* telescope results in groups of ten to thirty or more mid-infrared measurements spread over one or two days. The groups are separated by six month intervals. The first and sometimes the second group of observations include all four bands but later observations, made after the exhaustion of the solid hydrogen coolant, do not include the two longest wavelength bands, W3 and W4. As a result, the phase coverage is reasonably complete for most stars with periods less than about two days but becomes seriously incomplete for longer period stars, especially for W3 and W4; most stars with periods longer than ten days have measurements at two phases in W1 and W2 and one phase in W3 and W4. Thus, the *WISE* magnitudes for various stars and for various bands in the same star range from some that are good averages over the cycle to others that are only the mean of a few phases.

To assess the magnitude of the errors introduced by the phasing of the *WISE* photometry, we measured the amplitudes of the W1 and W2 light curves for 25 stars from our program

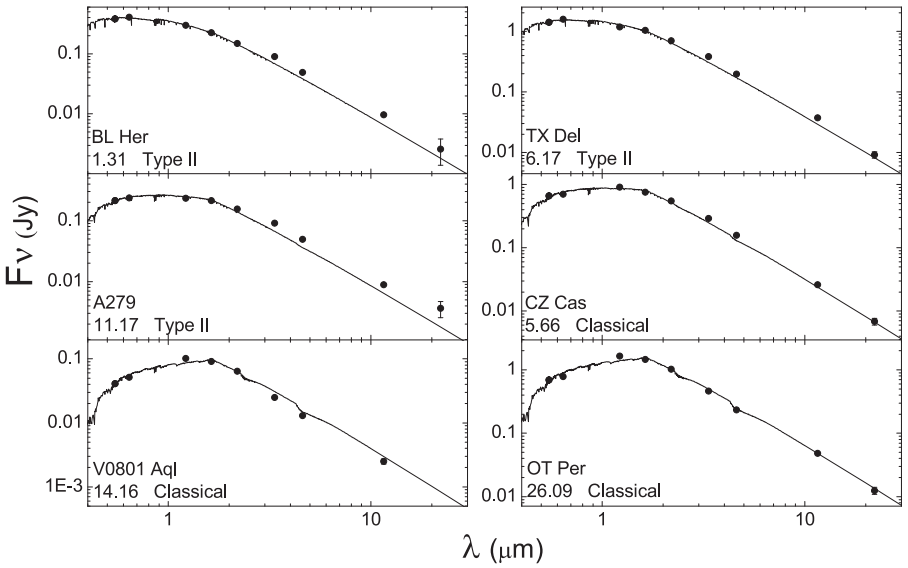

Figure 4. Spectral energy distributions for representative stars that lack detectable mid-infrared excesses (category D). The symbols are the same as for Figure 1.

that have V amplitudes greater than 0.6 mag and well sampled light curves. The average amplitudes are $\langle A_{W1}\rangle = 0.314 \pm 0.049$ and $\langle A_{W2}\rangle = 0.309 \pm 0.041$. We were unable to measure meaningful amplitudes for any of the stars in W3 and W4 due to poorer phase coverage and larger scatter but we expect them to be no larger than these values. Since there are at least two phases for many stars, the phase coverage of the *WISE* observations will result in scatter of a little more than ± 0.1 mag for the *WISE* magnitudes. This is considerably less than the effect of the single-phase JHK_S magnitudes so we will ignore it in this paper.

The main conclusions of this paper pertain to the stars with strong mid-infrared excesses (our category A described below) for which these errors have little effect. Thus, we will not attempt to improve on the near- and mid-infrared magnitudes here but will discuss them in a future paper where we will consider stars with weak mid-infrared emission in more detail.

3.1.4. Interstellar Extinction

As discussed in Section 2, the adopted values of E_{B-V} are neither as homogeneous nor as accurate as we would like. To test the effect on the fitting of the SEDs, we increased the reddenings for a number of stars by 0.25 mag and refitted the models to the observations. As expected, this increased the temperature of the fitted models significantly and raised the fitted fluxes in the mid-infrared. Consequently, reddening errors displace the model SEDs up or down relative to the four *WISE* fluxes that are much less affected by extinction. This is similar to the effect of using single-phase near-infrared fluxes as described in the previous section, Section 3.1.3. For that reason we can express the effect of extinction in terms of ΔJ and find that $\partial(\Delta J)/\partial(E_{B-V})$ ranges between 0.17 and 0.37 for various stars. This implies that extinction uncertainties as described in Section 2 may impact the values of ΔJ calculated below for individual stars by between 0.04 and 0.09 mag.

3.2. Identification of Stars with Excess Infrared Emission

Clearly it would be desirable to employ a quantitative measure for the mid-infrared emission. However, an examination of the energy distributions in Figures 1–4 shows that the form of the emission ranges widely among the various stars. For some in Figure 1, all four of the *WISE* bands are well above the photospheric level (e.g., IU Cyg and SZ Mon) while in others there is no significant excess in W1 and W2 but a strong excess is seen at longer wavelengths (e.g., NN Vul). The objects in Figure 2 differ from those in Figure 4 only in the slope of the mid-infrared points as discussed below. Because any excesses they might have are small, the types of errors described above in Sections 3.1.3 and 3.1.4 would vitiate the application of a quantitative measure to distinguish between them. Finally, the stars shown in Figure 3 all depart from the others in unique ways. Under these circumstances, an unambiguous quantitative measure of the emission is difficult to construct. Instead, we have examined the SEDs by eye and assigned them to four categories based on appearance.

3.2.1. Category A; Strong Mid-infrared Emission

For eight Cepheids, the mid-infrared flux is significantly above the photospheric level compared with the errors introduced by the limited phase coverage of the infrared data and the reddening uncertainties. Their SEDs are shown in Figure 1 and they are identified by the letter **A** in column (8) of Table 1.

Table 2 lists these stars, grouped by their Z-types, along with their periods in column (2), V amplitudes in column (3), metallicities from Schmidt et al. (2011) or Schmidt (2013) in column (4), intrinsic $(J-K)_o$ colors in column (5) and effective temperatures from the atmosphere fitting in column (6). The last two columns of Table 2 list parameters associated with the models described below.

3.2.2. Category B; Weak Mid-infrared Emission

Stars in category B have mid-infrared fluxes that fall close enough to the photospheric fluxes to be accounted for by the single-phase observations and reddening uncertainties. However, the *WISE* fluxes exhibit a shallower slope toward longer wavelengths than do the photospheric models. Examples are shown in Figure 2 and stars of this type are identified in column

Table 2
Stars With Strong Mid-infrared Emission, Category A

Star (1)	Period (2) (days)	A_V (3) (mag)	[Fe/H] (4)	$(J-K)_o$ (5) (mag)	$T_{\rm eff}$ (6) (K)	$r_{\rm min}$ (7) (AU)	$T_{\rm min}$ (8) (K)
			Type II Cepheids				
NSV 01272	4.17	1.99	…	1.33	4000	2.9	765
CC Lyr	24.23	0.63	…	0.48	6014	5.3	665
IU Cyg	31.35	1.02	…	0.72	5619	10.8	525
V0480 Lyr	52.2	0.45	−0.3	0.47	6042	4.0	1045
NSV 15229	96.	0.27[a]	…	0.34	8523	12.0	790
			Classical Cepheids				
QQ Per	11.19	0.61	0.2	0.45	5485	33.9	375
SZ Mon	16.33	1.28	−0.1	1.07	5543	17.2	575
NN Vul	30.82	1.05	…	0.32	5505	110.7	265

Note.
[a] This star showed no variation in the observations reported by Schmidt et al. (2009). The amplitude given here is based on photometry from the NSVS.

(8) of Table 1 by the letter **B**. As shown by Figures 1 and 2, there is a distinct difference between the category A and the category B stars; no ambigious cases were found in our sample.

The failure of the mid-infrared fluxes to follow the $1/\lambda^2$ dependence of the Rayleigh–Jeans tail of the SED is likely due to weak infrared emission. Some of the properties of these stars are listed in Table 3.

Table 3
Stars with Weak Mid-infrared Emission, Category B

Star (1)	Period (2) (days)	A_V (3) (mag)	[Fe/H] (4)	$(J-K)_o$ (5) (mag)	$T_{\rm eff}$ (6) (K)
		Type II Cepheids			
XX Vir	1.35	1.15	…	0.31	6179
A162	1.62	0.05	−0.7	0.35	7044
H012	5.10	0.16	…	0.69	4699
IX Cas	9.15	0.57	−0.1	0.42	6058
YZ Vir	14.47	1.22	…	0.46	5783
CS Cas	14.73	1.36	0.1	0.31	6396
V2631 Oph	15.19	1.29	…	0.48	5555
AL Sct	15.58	0.92	…	0.67	5413
V0478 Oph	16.35	1.00	…	0.42	5569
PP Aql	24.05	1.53	…	0.50	4622
TW Cap	28.56	1.36	−.9	0.43	5794
V0360 Cyg	70.36	1.14	−1.2	0.44	4809
		Classical Cepheids			
V0845 Her	15.5	0.91	…	0.61	5425

3.2.3. Category C; Anomalous Mid-infrared Fluxes

Figure 3 shows SEDs in which one or two of the *WISE* fluxes are above the trend of the other *WISE* fluxes after a possible vertical offset. In several cases one or two points at the longest wavelengths are high while in V0916 Aql the point from W1 at 3.4 μm is high. Some of the stars in this group may have cool circumstellar dust; others, like V0916 Aql, do not have an obvious explanation and may be due to errors in the data. We will not consider these stars as having demonstrated mass loss. They are indicated in Table 1 by the letter **C** in column (8).

3.2.4. Category D; Mid-infrared Fluxes Parallel to the Model SEDs

Figure 4 shows examples of SEDs that did not fit into categories A, B or C. In these stars, the mid-infrared fluxes fall along a line paralleling the model SED curve. Again, the vertical shifts can be explained by a combination of the use of single-phase near-infrared magnitudes and errors in the reddenings. To confirm this, we determined the shifts in the JHK_S magnitudes, ΔJ, and the corresponding values of ΔH and ΔK_S, required to bring the fitted mid-infrared model fluxes into agreement with the *WISE* fluxes.

Figure 5 shows the frequency distribution of ΔJ for all of the category D stars.[8] Since the near-infrared light curves are relatively symmetric around the median magnitude, single-phase observations should produce a distribution that is symmetric about $\Delta J = 0$ with scatter of $\sim\pm0.3$ mag. The obvious skew and offset of the distribution toward slightly smaller values of ΔJ might be accounted for by reddenings that are too small. With the available data, particularly the

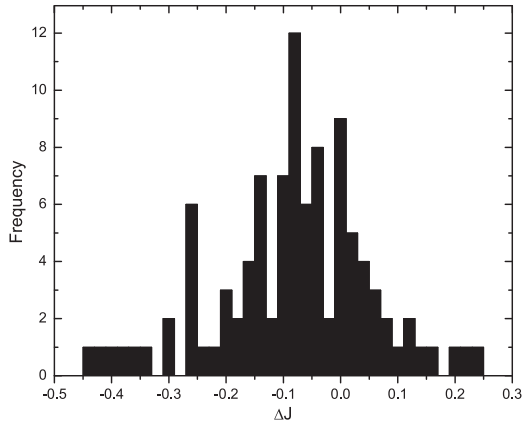

Figure 5. Distribution of the offsets of the near-infrared flux, ΔJ for all of the category D stars.

[8] A negative value of ΔJ corresponds to the *WISE* flux being above the model SED in Figure 4.

Table 4
The Distribution among Emission Categories

Category	*Z* Types				Category	VSX Types			
	Classical Cepheids		Type II Cepheids			Classical Cepheids		Type II Cepheids	
A	3	8%	5	5%	A	1	3%	5	9%
B	0	0%	13	14%	B	1	3%	10	17%
C	3	8%	8	8%	C	3	10%	4	7%
D	31	82%	69	73%	D	25	83%	39	67%
Total	37	…	95	…	Total	30	…	58	…

heterogeneous and inaccurate reddenings, we cannot separate the two effects.

We will consider the stars in this category to lack detectable mid-infrared excesses. They are indicated by the letter **D** in column (8) of Table 1.

3.3. The Occurrence of Mid-infrared Excesses

Table 4 shows the numbers of stars in each of the four infrared excess categories for the *Z*-type and the VSX classical and type II Cepheids. The most striking feature is that a large majority of both classical and type II Cepheids fall in categories C and D and, thus, lack detectable circumstellar dust. While approximately the same portion of each group exhibits strong excess emission (category A), marginal emission (category B) is much more prevalent among type II Cepheids. We expect the type II Cepheid metallicities to range from solar to about [Fe/H] = −2 (Schmidt 2013). Consequently, some of them will have high gas to dust ratios and thus weak infrared excesses for a given circumstellar mass. While this could result in a larger number of stars in category B, there are too few stars with metallicities (listed in column (4) of Tables 2 and 3) to discern a trend.

In Figure 6 we have plotted the amplitude, $(J - K)_o$ color and photospheric temperature against the period for the entire Cepheid sample. As indicated in the caption, the symbols distinguish the classical from type II Cepheids (following the *Z*-type classifications) and distinguish stars with different levels of emission. Stars with strong infrared excess all have periods longer than 11 days with a single exception. On the other hand, stars with marginal emission cover nearly the full range of periods of the complete sample. Although a few of the stars with emission are outliers in all three plots, there is no significant separation of stars with and without emission in any of the three panels.

This is puzzling. If mid-infrared emission is an indicator of mass loss, as often assumed, and if mass loss is driven by pulsation, we might expect that emission would be related to pulsational amplitude. However, stars with emission span the entire range of amplitudes in the sample. On the other hand if mass loss is related to location in the HR diagram, we should see a systematic separation in the colors and temperatures. Again this is not the case.

McAlary & Welch (1986) identified 61 classical and seven type II Cepheids from the third edition of the GCVS (Kukarkin et al. 1969) in the *Infrared Astronomical Satellite* (*IRAS*) *Point-Source Catalog*. Of the classical Cepheids, they found that 16, or 26%, had mid-infrared emission at some level. Five of the type II Cepheids, or 71%, were found to have strong emission

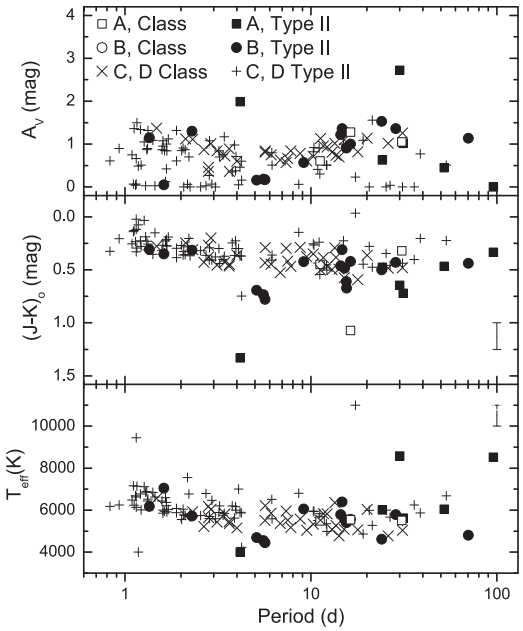

Figure 6. Several stellar properties plotted against pulsational period. Squares and circles represent stars in emission categories A and B, respectively. Filled symbols represent type II Cepheids and open symbols represent classical Cepheids. Plus signs and Xs represent type II and classical Cepheids, respectively, that have no infrared excess (categories C and D). The error bars at the right side of the middle and bottom panels show the effect of a change in E_{B-V} of ±0.25 mag.

that would have placed them easily in our category A. Even allowing for the relatively small number of stars, these numbers are much higher than the frequencies of emission listed in Table 4. Since McAlary & Welch (1986) selected Cepheids from the *IRAS* catalog, there is a bias favoring stars with strong infrared excesses. The effect is especially pronounced for the type II which are almost all fainter than the classical Cepheids.

To further explore this, we formed SEDs from the 2MASS and *WISE* photometry for the five type II Cepheids for which McAlary & Welch (1986) found infrared excesses. All of them except V0549 Sco showed excesses consistent with the SEDs in Figure 4 of McAlary & Welch (1986). The *WISE* catalog contains two stars within 1.3 arcmin of V0549 Sco that are more than five magnitudes brighter in W3. Given the sizes of the entrance apertures of the *IRAS* spectrometer, the apparent excess shown by McAlary & Welch (1986) is due to contamination from one or both of them.

We conclude that the higher incidence of emission that McAlary & Welch (1986) found is largely due to the selection of stars based on their being detected by *IRAS*.

4. THE SOURCE OF THE MID-INFRARED EMISSION

4.1. Mass Loss

To interpret the excess infrared emission of the category A stars, we attempted to fit mass-loss models to the infrared fluxes. This fitting is only feasible for stars with strong emission; the uncertainties introduced by the single-phase observations and the uncertainties of the reddenings vitiate the fitting for the stars with weak emission (category B).

We used Equation (2) from Neilson et al. (2010),

$$L_{\nu,\mathrm{Shell}} = 3\pi\frac{\langle a^2\rangle}{\langle a^3\rangle}\frac{\dot{M}_\mathrm{d}}{\bar{\rho}v_\mathrm{d}}Q_\nu^A \times \int_{r_c}^{\infty} B_\nu(T_\mathrm{d})[1 - W(r)]dr \quad (1)$$

where $L_{\nu,\mathrm{Shell}}$ is the monochromatic luminosity of the dust in the stellar wind, $\dot{M}_\mathrm{d}$ is the dust mass-loss rate, $\langle a^2\rangle$ and $\langle a^3\rangle$ are the means of the square and cube of the grain radii averaged over their distribution, $\bar{\rho}$ is the mean mass density of the dust grains, v_d is the dust velocity, T_d is the temperature of the dust grains, r is the distance from the star, $W(r) = [1 - \sqrt{1 - (r/R_*)^2}\,]/2$ is the geometric dilution factor of the radiation field, and r_c is the distance from the star at which T_d falls below the condensation temperature of the material comprising the dust.

Q_ν^A, the absorption efficiency parameter of the dust grains, depends on their composition. We did the analysis for three different compositions using Q_ν^A calculated as described by Laor & Draine (1993) and tabulated on B.T. Draine's web site[9] for silicate and graphite grains and from Kemper et al. (2002) for iron grains. Following Neilson et al. (2010) we have assumed a value for the average radii of the grains of $\langle a\rangle = 0.0059\ \mu$m based on the Mathis et al. (1977) distribution with radii between $a = 0.005$ and $0.25\ \mu$m.

We do not report the mass-losss rates, $\dot{M}_\mathrm{d}$, because we argue below that they are not meaningful. Thus, the values of $\langle a^2\rangle$, $\langle a^3\rangle$,$\bar{\rho}$, and v_d are not important here since they simply multiply $\dot{M}_\mathrm{d}$ in Equation (1).

Assuming that the dust temperature is determined by the balance between heating by the stellar radiation field and cooling by reradiation, it is given by

$$T_\mathrm{d} \cong T_\mathrm{eff}\left(\frac{2r}{R_*}\right)^{-0.5} \quad (2)$$

(Lamers & Cassinelli 1999, p. 163). T_eff and R_* are the effective temperature and radius of the star.

We determined the radii and luminosities of the stars using the PL relations of McNamara (1995) and Benedict et al. (2011) for the type II and classical Cepheids, resp., along with the colors and bolometric corrections of VandenBerg & Clem (2003) assuming the temperatures from column (6) of Table 2 and typical gravities and metallicities for each type of Cepheid. The monochromatic luminosities of the Cepheid photospheres were then obtained from the fitted models and the shell luminosities follow from them.

In principle, with this information, Equation (1) can be solved to derive $\dot{M}_\mathrm{d}$ from the excess flux above the photospheric level in each *WISE* band. To the degree that the model is a realistic representation of the conditions in the stellar wind, the four bands will give the same value for $\dot{M}_\mathrm{d}$.

Since the dust is densest and hottest at the condensation point, we expect that radiation from that location will dominate the emission. At the assumed condensation temperatures, $T_c = 1200$–1500 K for various grain compositions, the maximum of the Planck function falls in the range from 1.9 to 2.4 μm. Figure 1 shows that for some of the stars (in particular IU Cyg, QQ Per and SZ Mon) the infrared emission is weaker there than at longer wavelengths. Clearly there is little dust present near the condensation radius in those cases, a point that is reflected by the fact that Equation (1) yields very different values for $\dot{M}_\mathrm{d}$ for each of the *WISE* bands.

To adapt Equation (1) to this situation, we will assume that the circumstellar shell contains no dust closer than a distance of r_min from the star. Replacing the lower limit of the integral in Equation (1) with r_min and treating it as a free parameter to be determined along with $\dot{M}_\mathrm{d}$ so as to minimize the weighted standard deviation of the mass-loss rates from the four *WISE* bands, we obtained a value for r_min and $\dot{M}_\mathrm{d}$ for each star. Using these values, we calculated the best fit SED for the shell with Equation (1).

Using silicate grains, no satisfactory fit could be obtained. This arises from the large increase in the silicate Q_ν^A at wavelengths longward of 6 μm (see Lamers & Cassinelli 1999, p. 158) that produces the well-known silicate bumps at 9.7 and 20 μm in many stars with dusty winds (see, for example, Bedijn 1987). This is confirmed by an examination of Figure 1 where no excess emission is apparent above the fitted curve (using graphite) at 10 μm. This does not rule out a significant contribution from silicate dust since, for example, the 9.7 μm silicate feature would be suppressed if the grains were much larger than assumed; if $a \gtrsim 10\ \mu$m, Q_ν^A exhibits no discrete features.

Q_ν^A for either graphite or iron grains produced reasonably good fits to the SEDs although those with graphite were slightly better. We will use the results from graphite to illustrate the following discussion but it must be emphasized that the composition of the grains cannot be determined with the present data and models.

The total SEDs of the shell and the star calculated for graphite are plotted in Figure 1 as light lines. The match between the model fluxes and the observations is quite satisfactory considering the many assumptions and idealizations that went into the derivation and application of Equation (1). Columns (7) and (8) of Table 2 list the minimum radii of the dust shells, r_min, and the dust temperatures, T_min, at that location.

It is unlikely that the gas could reach temperatures well below the condensation temperature of the grains without detectable grains forming. Thus the low values for T_min in Table 2 strongly suggest that there is not significant gas closer to the star than r_min; the circumstellar shell has a void around the star in both the gas and the dust density.

If, following Neilson et al. (2010), we assume an expansion velocity of $v_\mathrm{d} = 100\ \mathrm{km\ s^{-1}}$, the shell will cover the largest inner shell radius in Table 2, 111 AU for NN Vul, in less than 6

[9] http://www.astro.princeton.edu/~draine/dust/dust.diel.html

years. Given this short time scale, the circumstellar shells will be dispersed much too quickly to allow us observe them if they are not replenished by a wind from the star. Furthermore, the *IRAS* measurements of IU Cyg (open circles in Figure 1) agree with the *WISE* measurements even though they were taken about 27 years earlier. Thus, the assumption that the mid-infrared emission of these stars is due to a stellar wind is inconsistent with the observations; the circumstellar gas and dust must be relatively stationary relative to the star.

It should be noted that the conclusions of the previous paragraph are little affected by the various assumptions relating to the expansion velocity and its constancy, the assumed dust properties (aside from Q_ν^A), or even the distribution of the dust in the shell. The value of $R_{\rm min}$ and $T_{\rm min}$ depend mostly on the temperature variation given by Equation (2) which is just based on the radiative equilibrium of the grains in the stellar radiation field.

We conclude that the excess emission in the mid-infrared is not indicative of mass loss. Rather it is due to stationary dust at distances of the order of about 3–110 AU from the star.

4.2. Other Possible Sources of Circumstellar Matter

If the circumstellar dust is not the product of mass loss, then what is its source? Kervella et al. (2012) argued that the reflection nebula surrounding the Cepheid RS Pup may be either the remnants of the cloud from which the star formed or unrelated interstellar material in which it happens to be embedded currently. We could speculate that one of these scenarios might also apply to some of our category A stars. While this may be a possibility for the classical Cepheids, it is less likely for the type II Cepheids due to their greater ages and generally larger distances from the Galactic Plane. We cannot investigate this with the existing data but searches for circumstellar clouds with infrared imagery or interferometry might provide some insight. However, the difficulties in establishing that the dust in the Pleaides cluster is environmental (see, for example, the discussion by Herbig 1996) suggests that a definitive answer will be elusive.

A second possibility is the presence of a binary companion that can have important consequences for circumstellar material. It appears that binary companions are likely to be common among both classical and type II Cepheids (Szabados 2003; Welch 2012; Evans et al. 2015). Among the classical Cepheids in our list only five, KL Aql, V916 Aql, AN Aur, V0351 Cep, and CP Cep, are listed in Laszlo Szabados' database of Cepheid binaries[10] while only two type II Cepheids in our sample have been identified as having close companions, IX Cas and TX Del (Welch 2012). Of these seven stars, six are in our category D (no detectable infrared excess) and one, IX Cas, is in category B. This does not support the suggestion that binarity plays a role in the infrared excesses but further investigation must await more detailed studies of individual stars from our program.

Both environment and binarity as factors in the excess infrared emission are consistent with our conclusion that the circumstellar dust does not represent mass loss and with the lack of any apparent relationship with the stellar properties as shown in Figure 6. On the other hand, the objections to both scenarios are serious. A resolution of this problem will have to await further investigation.

[10] http://www.konkoly.hu/CEP/intro.html

5. CONCLUSIONS

1. Excess mid-infrared emission is not detectable in a large majority of Cepheids, 90% or more of classical Cepheids and more than three-fourths of type II Cepheids, depending on how individual stars are classified.
2. The presence of emission is not related to either pulsational amplitude or effective temperature but, with one exception, strong emission is only found in stars with periods longer than 11 days.
3. For the stars with strong mid-infrared emission, a stellar wind model does not fit the observed SEDs. We conclude that the emission arises from stationary dust at distances of a few to about 110 AU from the stars.

The author is grateful to Hilding Neilson, Douglas Welch, and the referee, Dr. Greg Sloan, for comments that helped improve the contents of this paper significantly. This publication makes use of data products from the *Wide-field Infrared Survey Explorer*, which is a joint project of the University of California, Los Angeles, and the Jet Propulsion Laboratory/California Institute of Technology, funded by the National Aeronautics and Space Administration. This publication makes use of data products from the Two Micron All Sky Survey, which is a joint project of the University of Massachusetts and the Infrared Processing and Analysis Center/California Institute of Technology, funded by the National Aeronautics and Space Administration and the National Science Foundation. This research has made use of the International Variable Star Index (VSX) database, operated at AAVSO, Cambridge, Massachusetts, USA.

REFERENCES

Barmby, P., Marengo, M., Evans, N. R., et al. 2011, AJ, 141, 42
Bedijn, P. J. 1987, A&A, 186, 136
Benedict, G. F., McArthur, B. E., Feast, M. W., et al. 2011, AJ, 142, 187
Bohm-Vitense, E., & Love, S. G. 1994, ApJ, 420, 401
Castelli, F., & Kurucz, R. L. 2003, in IAU Symp. 210, Modeling of Stellar Atmospheres, ed. N. E. Piskunov, W. W. Weiss & D. F. Gray (San Francisco, CA: ASP), A20
Deasey, H., & Butler, C. J. 1986, Natur, 320, 726
Deasey, H. P. 1988, MNRAS, 231, 673
Evans, N. R., Berdnikov, L., Lauer, J., et al. 2015, AJ, 150, 13
Fitzpatrick, E. L. 1999, PASP, 111, 63
Fernie, J. D. 1990, ApJS, 17, 153
Herbig, G. H. 1996, AJ, 111, 1241
Inno, L., Matsunaga, N., Romaniello, M., et al. 2015, A&A, 576, A30
Kemper, F., de Koter, A., Waters, L. B. F. M., Bouwman, J., & Tielens, A. G. G. M. 2002, A&A, 384, 585
Kervella, P., Merand, A., & Gallennne, A. 2009, A&A, 498, 425
Kervella, P., Merand, A., Szabados, L., et al. 2012, Msngr, 150, 46
Kukarkin, B. V., Kholopov, P. N., Efremov, Yu. N., et al. 1969, General Catalog of Variable Stars (3rd ed.; Moscow: Sternberg State Astronomical Institute, Moscow State University)
Lamers, H. J. G. L. M., & Cassinelli, J. P. 1999, Introduction to Stellar Winds (Cambridge: Cambridge Univ. Press)
Laor, A., & Draine, B. T. 1993, ApJ, 402, 441
Marengo, M., Evans, N. R., Barmby, P., et al. 2010, ApJ, 725, 2392
Mathis, J. S., Rumpl, W., & Nordsieck, K. H. 1977, ApJ, 217, 425
Matsunaga, N., Feast, M. W., Kawadu, T., et al. 2013, MNRAS, 429, 385
Matthews, L. D., Marengo, M., Evans, N. R., & Bono, G. 2012, ApJ, 744, 53
McAlary, C. W., & Welch, D. L. 1986, AJ, 91, 1209
McNamara, D. H. 1995, AJ, 109, 2134
Merand, A., Aufdenberg, J. P., Kervella, P., et al. 2007, ApJ, 664, 1093
Merand, A., Kervella, P., Conde du Foresto, V., et al. 2006, A&A, 453, 155
Nardetto, N., Groh, J. H., Kraus, S., Millour, F., & Gillet, D. 2008, A&A, 489, 1263
Neilsen, H. R., Langer, N., Engle, S. G., Buinan, E., & Izaard, R. 2012, ApJL, 760, L18

Neilson, H. R., & Lester, J. B. 2008, ApJ, 684, 569
Neilson, H. R., Ngeow, C.-C., Kanbur, S. M., & Lester, J. B. 2009, ApJ, 692, 81
Neilson, H. R., Ngeow, C.-C., Kanbur, S. M., & Lester, J. B. 2010, ApJ, 716, 1136
Schlafly, E. F., & Finkbeiner, D. P. 2011, ApJ, 737, 103
Schlegel, D. J., Finkbeiner, D. P., & Davis, M. 1998, ApJ, 500, 525
Schmidt, E. G. 2013, AJ, 146, 61
Schmidt, E. G., Hemen, B., Rogalla, D., & Thacker-Lynn, L. 2009, AJ, 137, 4598
Schmidt, E. G., Johnston, D., Langan, S., & Lee, K. M. 2004, AJ, 128, 1748
Schmidt, E. G., Johnston, D., Langan, S., & Lee, K. M. 2005a, AJ, 129, 2007
Schmidt, E. G., Johnston, D., Langan, S., & Lee, K. M. 2005b, AJ, 130, 832
Schmidt, E. G., Langan, S., Rogalla, D., & Thacker-Lynn, L. 2007, AJ, 133, 665
Schmidt, E. G., & Parsons, S. B. 1984, ApJ, 279, 202
Schmidt, E. G., Rogalla, D., & Thacker-Lynn, L. 2011, AJ, 141, 53
Skrutskie, M. F., Cutri, R. M., Steining, R., et al. 2006, AJ, 131, 1163
Szabados, L. 2003, in ASP Conf. Ser. 298, GAIA Spectroscopy, Science and Technology, ed. U. Munari (San Francisco, CA: ASP), 237
VandenBerg, D. A., & Clem, J. L. 2003, AJ, 126, 778
Welch, D. L. 2012, JAVSO, 40, 492
Welch, D. L., Wieland, F., McAlary, C. W., et al. 1984, ApJS, 54, 547
Wright, E. L., Eisenhardt, P. R. M., Mainzer, A. K., et al. 2010, AJ, 140, 1868